

Elementary excitations and specific heat in quantum sine-Gordon spin chain KCuGaF₆

Izumi Umegaki, Toshio Ono, Hidekazu Tanaka^a, Masaki Oshikawa^b, Hiroyuki Nojiri^c

^aDepartment of Physics, Tokyo Institute of Technology, Oh-okayama, Meguro-ku, Tokyo 152-8551, Japan

^bInstitute for Solid State Physics, The University of Tokyo, Kashiwanoha, Kashiwa, Chiba 277-8581, Japan

^cInstitute for Material Research, Tohoku University, Katahira, Aoba-ku, Sendai 980-8577, Japan

Abstract

Elementary excitations of an $S=1/2$ antiferromagnetic Heisenberg chain KCuGaF₆ were investigated through specific heat and electron spin resonance (ESR) measurements. In this compound, a staggered field is induced perpendicular to the external field because of the alternating g tensor and the Dzyaloshinsky-Moriya interaction with an alternating \mathbf{D} vector. Such a spin system can be mapped onto the quantum sine-Gordon (SG) model, when subjected to the external magnetic field. Specific heat shows clear evidence of the field-induced gap, which is related to the elementary excitations, solitons and breathers, characteristic of the quantum SG model. $q=0$ excitations originated from solitons and breathers were directly observed by high-frequency high-field ESR. These experimental results are well described by the quantum SG field theory.

Keywords: antiferromagnetic Heisenberg chain, field-induced gap, quantum sine-Gordon model, specific heat, ESR, KCuGaF₆

1. Introduction

The study of $S=1/2$ antiferromagnetic Heisenberg chain (AFHC) has a long history. The ground state energy, dispersion relation for spinon excitations and magnetization process were exactly calculated using the Bethe Ansatz [1, 2, 3]. The energy of the lowest spinon excitation called des Cloizeaux-Pearson (dCP) mode is given by $E(q) = (\pi/2)J|\sin q|$, which is a factor $\pi/2$ as large as the result of the linear spin wave theory [2]. The dCP mode is gapless at wave vectors $q=0$ and π . Under magnetic field, the gapless excitations occur at incommensurate wave numbers $q = \pm 2\pi m(H) (\equiv \pm q_0)$ and $\pi \pm q_0$ in addition to at $q=0$ and π , where $m(H)$ is the dimensionless magnetization per site [4].

Oshikawa and Affleck [5, 6] discussed the excitations in $S=1/2$ AFHC under the staggered magnetic field h that is induced perpendicular to the external magnetic field H . The Hamiltonian of such system is expressed as

$$\mathcal{H} = \sum_i \left\{ JS_i \cdot S_{i+1} - g\mu_B HS_i^z - (-1)^i g\mu_B h S_i^x \right\}. \quad (1)$$

In real magnetic materials, the alternating g tensor and the Dzyaloshinsky-Moriya (DM) interaction with the alternating \mathbf{D} vector can produce the staggered field. Using the bosonization technique, they [5, 6] argued that the model (1) can be mapped onto the quantum sine-Gordon (SG) model with Lagrangian density

$$\mathcal{L} = \frac{1}{2} \left[\left(\frac{\partial \phi}{\partial t} \right)^2 - (vJ)^2 \left(\frac{\partial \phi}{\partial x} \right)^2 \right] + hC \cos(2\pi R\tilde{\phi}), \quad (2)$$

where ϕ is a canonical Bose field, $\tilde{\phi}$ is the dual field, R is the compactification radius, v is the dimensionless spin velocity and C is a coupling constant. The first term corresponds to

the free boson field that represents Tomonaga-Luttinger (TL) liquid. The second term expresses the nonlinear effect due to the staggered field. Oshikawa and Affleck [5, 6] showed that all the gapless points at zero field become gapped in finite field as shown in Fig. 1, and that the magnitude of the gap is proportional to $H^{2/3}$ for $g\mu_B H/J \ll 1$. Their result gives a good description of the unexpected field-induced gap observed in $\text{Cu}(\text{C}_6\text{H}_5\text{COO})_2 \cdot 3\text{H}_2\text{O}$ abbreviated as Cu benzoate [7].

Besides Cu benzoate [7, 8, 9], PM-Cu(NO₃)₂·(H₂O)₂ (PM = pyrimidine) [10, 11] and Yb₄As₃ [12, 13] have been known as the quantum SG systems. In these compounds, the exchange interaction is order of 10 K and the proportional coefficient $c_s = h/H$ is rather small, $c_s = 0.08$ [9, 11]. For the deep understanding of the systems represented by the model (1), new compounds having different interaction constants are necessary. In this paper, we introduce KCuGaF₆, which can be described by the model (1) with a large exchange interaction $J/k_B \simeq 100$ K and a large proportional coefficient, $c_s \simeq 0.2$ [14].

KCuGaF₆ belongs to a pyrochlore family represented by a chemical formula AMM'F₆, where A is a monovalent alkaline ion, and M and M' are divalent and trivalent metal ions, respectively. M²⁺ and M'³⁺ ions form a pyrochlore lattice. According to the combination of the M and M' ions, the system shows a variety of physical properties. KCuGaF₆ has a monoclinic structure of space group $P2_1/c$ [15]. The lattice parameters at room temperature are $a = 7.2856 \text{ \AA}$, $b = 9.8951 \text{ \AA}$, $c = 6.7627 \text{ \AA}$ and $\beta = 93.12^\circ$. Figure 2 shows the crystal structure of KCuGaF₆. Cu²⁺ and Ga³⁺ ions are arranged to form chains along the c and a axes, respectively. The chains of Cu²⁺ ions with spin-1/2 are separated by the chains of nonmagnetic Ga³⁺ ions. Cu²⁺ is surrounded octahedrally by six F⁻ ions, and CuF₆ octahedra are elongated perpendicular to the chain direction parallel to the c axis owing to the Jahn-Teller effect. The elongated axes

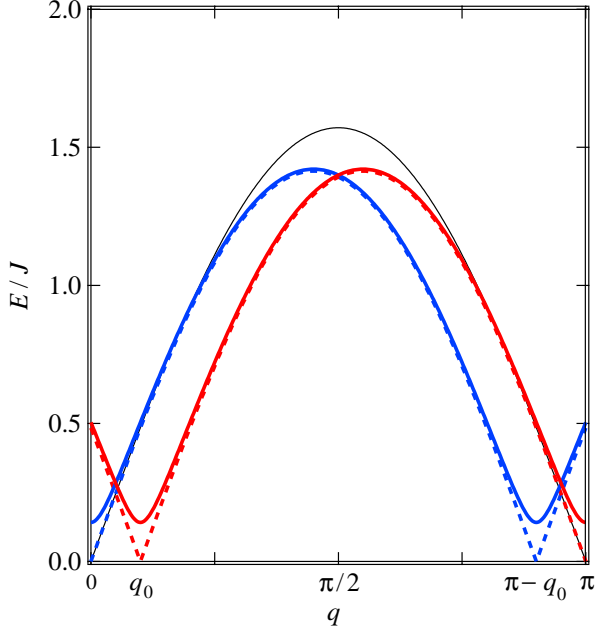


Figure 1: Illustration of the lowest energy excitations of model (1) under nonzero magnetic field with finite staggered field (thick solid lines). Excitations at $q=0, \pi$ and incommensurate wave numbers $q=\pm q_0$ and $\pi\pm q_0$ have finite gaps. The excitations without staggered field are denoted by dashed lines. Thin solid line is the dCP mode at zero field.

alternate along the c axis. For this reason, the hole orbitals of Cu^{2+} ions are linked along the chain direction through the p orbitals of F^- ions. The bond angle α of the exchange pathway $\text{Cu}^{2+} - \text{F}^- - \text{Cu}^{2+}$ is $\alpha = 129^\circ$. This large bond angle produces the strong antiferromagnetic exchange interaction of the order of 10^2 K. Thus, KCuGaF_6 can be expected to be $S = 1/2$ AFHC, which can be verified from the fact that no magnetic ordering is observed down to 0.5 K [16].

In KCuGaF_6 , the local principal axes of CuF_6 octahedra are tilted alternately along the c axis, as shown in Fig. 2. This leads to the staggered inclination of the principal axes of the g tensor. The DM interaction of the form $\mathbf{D}_i \cdot [\mathbf{S}_i \times \mathbf{S}_{i+1}]$ also exist, because there is no inversion center at the middle point of two adjacent spins along the c axis. Therefore, the magnetic model of KCuGaF_6 in external magnetic field \mathbf{H} is expressed as

$$\mathcal{H} = \sum_i \{JS_i \cdot S_{i+1} - \mu_B \mathbf{S}_i \mathbf{g}_i \mathbf{H} + \mathbf{D}_i \cdot [\mathbf{S}_i \times \mathbf{S}_{i+1}]\}. \quad (3)$$

The staggered g tensor at the i -th spin site is written as

$$\mathbf{g}_i = \mathbf{g}_u + (-1)^i \mathbf{g}_s, \quad (4)$$

where \mathbf{g}_u is the uniform g tensor without nondiagonal term that is common to all the spin sites and \mathbf{g}_s is the staggered g tensor with nondiagonal terms only. The staggered g tensor contributes to the staggered magnetic field $\mathbf{h}_i^s = (-1)^i \mathbf{g}_s \mathbf{H} / g'$ that is induced perpendicular to the external magnetic field \mathbf{H} , where g' is the uniform g factor for the staggered field direction. At present, details of the g tensor are not clear, because no ESR signal at conventional frequencies (9 or 24 GHz) is observed

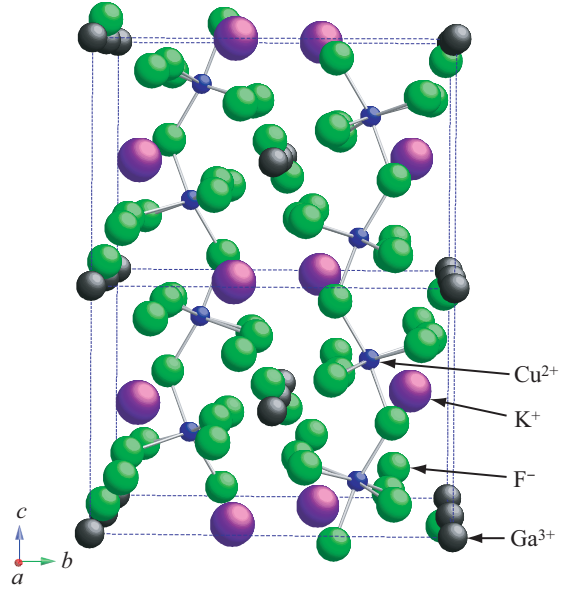


Figure 2: Crystal structure of KCuGaF_6 viewed along the a axis. Cu^{2+} ions with spin-1/2 form chains along the c axis.

at room temperature owing to large linewidth, which should be ascribed to the DM interaction discussed below.

The \mathbf{D}_i vector of the DM interaction is an axial vector given by the nondiagonal components of the angular momenta of adjacent magnetic ions. Since there is the c glide plane at $\pm b/4$, the ac plane component of the \mathbf{D}_i vector alternates along the chain direction, but the b component does not. Thus, the \mathbf{D}_i vector is expressed as $\mathbf{D}_i = ((-1)^i D_x, D_y, (-1)^i D_z)$, where the x , y and z axes are chosen to be parallel to the a^* ($\perp b, c$), b and c axes, respectively. If the y component D_y is negligible, then the \mathbf{D}_i vector is expressed as $\mathbf{D}_i = (-1)^i \mathbf{D}$. According to the argument by Affleck and Oshikawa [6], the effective staggered field \mathbf{h}_i acting on \mathbf{S}_i is approximated as

$$\mathbf{h}_i \simeq \frac{(-1)^i}{g'} \left[\frac{g}{2J} \mathbf{g}_s \mathbf{H} + \mathbf{H} \times \mathbf{D} \right]. \quad (5)$$

Equation (5) means that the staggered field \mathbf{h}_i is induced perpendicular to the external magnetic field \mathbf{H} and its magnitude is proportional to H . Hence, the effective Hamiltonian of the present system can be written as eq. (1). For simplification, we set $g' = g$ hereafter, and we rewrite $(g'/g)\mathbf{h}_i$ as \mathbf{h}_i .

The arrangement of this paper is as follows: In section 2, we summarize the elementary excitations in quantum SG model. The experimental procedures are presented in section 3. The results of the specific heat and ESR measurements and discussion are presented in section 4. Section 5 is devoted to the conclusion.

2. Elementary excitations in quantum SG model

In the quantum SG model, low-energy elementary excitations are composed of solitons, antisolitons and their bound

states called breathers. Figure 3 illustrates low-energy excitations around $q=0$ for $h \neq 0$ (solid lines) and $h=0$ (dashed lines). Because of the staggered field h induced by the external magnetic field, the gapless excitations at $q=0$ and $\pm q_0$ for $h=0$ have finite gaps. The soliton mass M_s corresponds to the excitation energy at $q = \pm q_0$ and $\pi \pm q_0$. The analytical form of M_s given by Essler *et al.* [17] is expressed as

$$M_s = \frac{2vJ}{\sqrt{\pi}} \frac{\Gamma\left(\frac{\xi}{2}\right)}{\Gamma\left(\frac{1+\xi}{2}\right)} \left[\frac{\Gamma\left(\frac{1}{1+\xi}\right)}{\Gamma\left(\frac{\xi}{1+\xi}\right)} \frac{c\pi g\mu_B H}{2Jv} c_s \right]^{(1+\xi)/2}, \quad (6)$$

where v is the dimensionless spin velocity, ξ is a parameter given by $\xi = [2/(\pi R^2) - 1]^{-1}$ and c is a parameter depending on magnetic field. The field dependences of these parameters are shown in the literature [6, 17, 18]. For $H \rightarrow 0$, $v \rightarrow \pi/2$, $\xi \rightarrow 1/3$ and $c \rightarrow 1/2$, and thus, $M_s \propto H^{2/3}$ as shown by Oshikawa and Affleck [5, 6]. Equation (6) is applicable in a wide magnetic field range up to the saturation field $H_s = 2J/g\mu_B$.

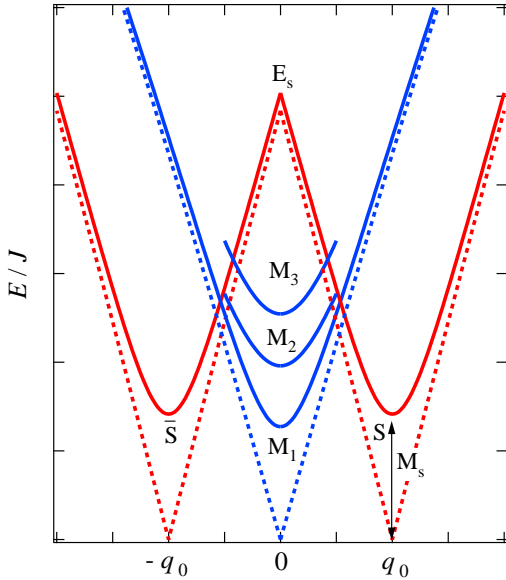


Figure 3: Structure of low-energy excitations around $q=0$. Soliton, antisoliton, soliton resonance and three breathers are labeled as S , \bar{S} , E_s and $M_1 \sim M_3$, respectively. The excitations without staggered field are denoted by dashed lines.

The breathers correspond to the excitations at $q=0$ and π and have hierarchical structures labeled by integer $n (= 1, 2, \dots)$. The mass of the n -th breather can be written as

$$M_n = 2M_s \sin\left(\frac{n\pi\xi}{2}\right). \quad (7)$$

The number of breathers is limited by $n \leq [\xi^{-1}]$ [6]. In our experimental field range, $g\mu_B H/J < 0.5$, breathers up to the third order can exist. In general, the mass of the first breather M_1 is smaller than the soliton mass M_s , because $\xi < 1/3$ in finite external field. If the SU(2) symmetry is conserved, then $\xi = 1/3$ and $M_1 = M_s$.

In electron spin resonance experiment (ESR), we can observe only $q=0$ excitations. Thus, the soliton and antisoliton cannot be observed directly by ESR. Instead, we can observe a soliton resonance labeled E_s in Fig. 3, which corresponds to the excitation energy at $q=0$ on the excitation branch connected to the soliton and antisoliton at $q = \pm q_0$ [6, 11]. The condition of the soliton resonance is written by

$$E_s \simeq \sqrt{M_s^2 + (g\mu_B H)^2}. \quad (8)$$

From the field for the soliton resonance, we can evaluate the soliton mass M_s .

Within the framework of the linear spin wave theory, we have only two modes for $q=0$ excitations, which are expressed as

$$E_- \simeq \sqrt{4Jc_s H S}, \quad E_+ \simeq \sqrt{\Delta^2 + (g\mu_B H)^2}, \quad (9)$$

where the gap is given by $\Delta = E_-$. The modes E_- and E_+ correspond to the first breather M_1 and soliton resonance E_s , respectively. For the number of excitations and the field dependence of the gap, there is the significant difference between the results of the quantum SG field theory and the conventional linear spin wave theory.

3. Experimental

KCuGaF₆ single crystals were grown by both vertical and horizontal Bridgman methods from the melt of a stoichiometry mixture of KF, CuF₂ and GaF₃ packed into a Pt tube. The materials were dehydrated by heating in vacuum at about 100 °C for three days. After the dehydration, one end of the Pt tube was welded and the other end was tightly folded with pliers. The temperature at the center of the furnace was set at 850 °C, and the lowering rate was 2~3 mm/h. KCuGaF₆ seems to show incongruent melting. Transparent light-pink crystals with a typical size of $3 \times 3 \times 3$ mm³ were obtained. These crystals were identified as KCuGaF₆ by X-ray powder diffraction analysis.

Crystallographic a , b and c axes were determined by X-ray single-crystal diffraction. Crystals are cleaved along the (1, 1, 0) plane. Magnetic susceptibilities measured for magnetic field parallel to these three axes are largely anisotropic below 50 K, which can be ascribed to the DM interactions [19]. The magnitude of the susceptibility below 50 K is given as $\chi_c > \chi_b > \chi_a$. Thus, these crystallographic axes can be determined from the susceptibility measurements.

The high-frequency, high-field ESR measurements were performed in the frequency range of 135 – 761.6 GHz using the terahertz electron spin resonance apparatus (TESRA-IMR) [9] at the Institute for Material Research, Tohoku University. The temperature of the sample was lowered to 0.5 K using liquid ³He in order to suppress the finite temperature effect. Magnetic field up to 30 T was applied with a multilayer pulse magnet. FIR lasers, backward traveling wave tubes and Gunn oscillators were used as light sources. ESR absorption signals were collected for $H \parallel a$, $H \parallel b$, $H \parallel c$ and $H \perp (1, 1, 0)$. Specific heat measurements were carried out down to 0.35 K in magnetic fields of up to 9 T using a physical property measurement system (Quantum Design PPMS) by the relaxation method.

4. Results and discussion

4.1. Electron spin resonance measurement

Because ESR is the most powerful tool for detecting $q=0$ excitations with high resolution, we performed high-frequency ESR measurements combined with pulsed high magnetic field at 0.5 K to observe elementary excitations in KCuGaF_6 . Due to a large exchange interaction $J/k_B = 103$ K, we are able to observe elementary excitations in the relatively low-field region over a wide energy range as compared with copper benzoate [8, 9] and $\text{PM-Cu}(\text{NO}_3)_2 \cdot (\text{H}_2\text{O})_2$ [11]. Thus, KCuGaF_6 is considered to be useful for comprehensive study of the elementary excitations in the quantum SG system.

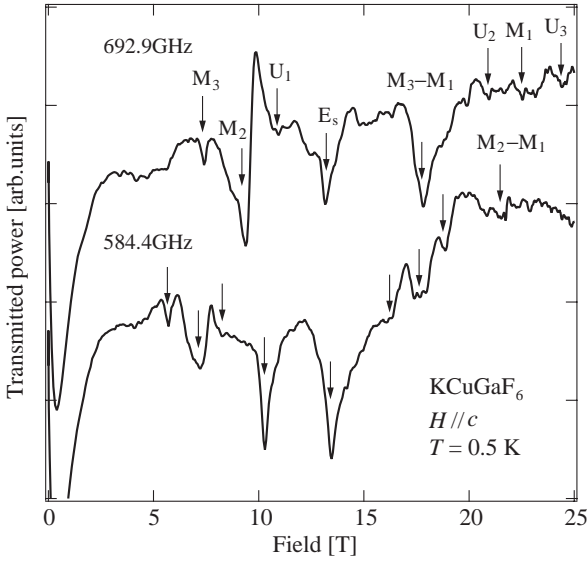


Figure 4: Examples of ESR spectra obtained at 0.5 K for $H \parallel c$.

Since ESR detects the $q=0$ excitations, the excitations labeled M_1 , M_2 , M_3 and E_s in Fig. 3 can be observed. We can also evaluate the soliton mass indirectly from the field for the soliton resonance E_s . In Fig. 4, we show examples of ESR spectra obtained at $T = 0.5$ K for $H \parallel c$. Arrows indicate resonance fields in each frequency. Absorption signals observed upon sweeping field both up and down were determined as intrinsic resonance signals. In addition to the case for $H \parallel c$, we measured ESR spectra for $H \parallel b$, $H \perp (1, 1, 0)$ and $H \parallel a$. In these four different field directions, we observed as many as about ten resonance modes. This result is apparently different from the picture of the conventional linear spin wave theory that is composed of only two excitation modes. Labels in Fig. 4 denote the assignment of the modes, which will be shown below. Figure 5 shows the frequency vs field diagrams that summarizes the resonance data for $H \parallel c$ and $H \parallel a$. The resonance modes labeled as E_s and M_n ($n = 1 \sim 3$) were assigned as soliton resonance and breathers from their resonance conditions calculated using eqs. (6)–(8) with exchange constant $J/k_B = 103$ K and proportionality coefficient $c_s = h/H$ shown below. For $H \parallel c$, $H \parallel b$, $H \perp (1, 1, 0)$, and $H \parallel a$, the proportionality coefficient

$c_s = 0.18, 0.16, 0.06$, and 0.03 , respectively. The soliton resonance and the breathers up to the third order are the main excitations predicted by the quantum SG field theory. In KCuGaF_6 , all of these excitations were clearly observed for four different field directions. As shown in Fig. 5, the experimental results are successfully described by the quantum SG field theory with only adjustable parameter c_s . In these calculations, we used $g = 2.32$ for $H \perp (1, 1, 0)$, which was determined by the present ESR measurement at $T \sim 60$ K. The g factors used for $H \parallel a$, $H \parallel b$ and $H \parallel c$ are $g = 2.28, 2.36$ and 2.12 , respectively, which were determined from the uniform magnetic susceptibilities χ_u at room temperature, assuming that χ_u/g^2 is constant.

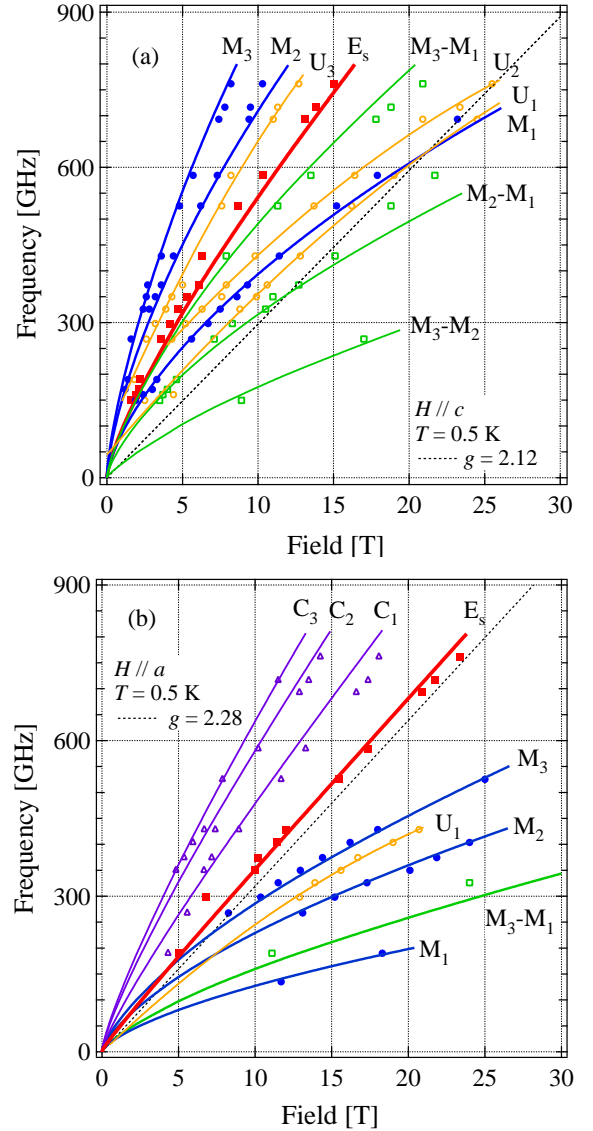


Figure 5: Frequency vs field diagrams for (a) $H \parallel c$ and (b) $H \parallel a$. Symbols denote experimental results and thick solid lines are resonance conditions calculated from the quantum SG field theory with $c_s = 0.18$ and 0.03 , respectively.

In Fig. 6, we compare the field dependence of the first breather mass M_1 observed for four different field directions.

In the present field range $g\mu_B H/J < 0.4$, $M_1 \approx 0.9M_s$. The proportionality coefficient c_s reaches a maximum (0.18) for $H \parallel c$ and a minimum (0.03) for $H \parallel a$. Such a large proportionality coefficient as observed for $H \parallel c$ has not been observed in other SG systems. The magnitude of c_s is almost the same for $H \parallel c$ and $H \parallel b$. Since the angle between the b axis and the line perpendicular to the $(1, 1, 0)$ plane is $\theta_0 = 53.6^\circ$, the first breather mass M_1 for $H \perp (1, 1, 0)$ is approximately expressed as $M_1(H \parallel a) + \Delta M_1 \cos^2 \theta_0$, where $\Delta M_1 = M_1(H \parallel b) - M_1(H \parallel a)$. This indicates that for $H \parallel ab$ plane, $M_1 \approx M_1(H \parallel a) + \Delta M_1 \cos^2 \theta$, where θ is the angle between the b axis and the external field.

The intensities of the main resonance modes, the soliton resonance E_s and the breathers M_n , are of the same order. These two excitations occur under different conditions for the oscillating magnetic field H_1 of the submillimeter wave. The soliton resonance occurs when H_1 perpendicular to the external field H , while breathers are excited when H_1 is parallel to H [20]. Since unpolarized submillimeter wave propagates in a light pipe whose diameter is larger than its wavelength, the oscillating magnetic field has components both parallel and perpendicular to the external field. Consequently, both the soliton resonance and the breathers can be observed at once in the present experiments.

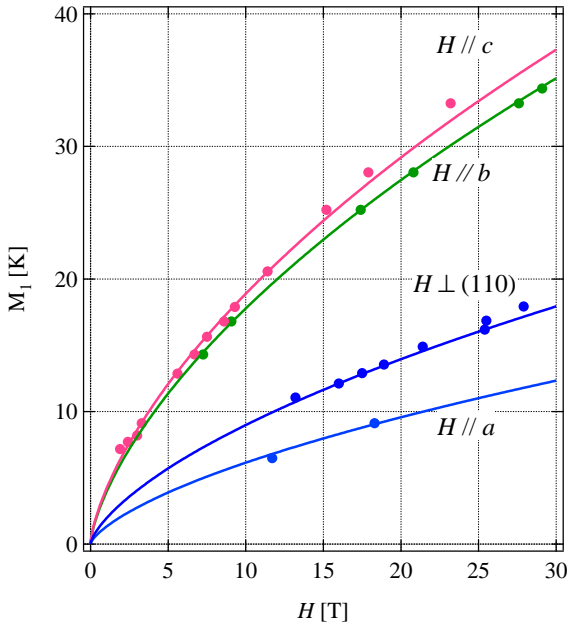


Figure 6: Mass of the first breather M_1 obtained for $H \parallel c$, $H \parallel b$, $H \perp (1, 1, 0)$, and $H \parallel a$. Symbols denote experimental results and solid lines are resonance conditions calculated from eqs. (6) and (7) with $c_s = 0.18, 0.16, 0.06$, and 0.03 , respectively.

In addition to the main elementary excitations E_s and M_n ($n = 1 \sim 3$), some resonance modes were observed, as shown in Figs. 4 and 5. We will discuss below these additional modes. The excitation energies of the modes labeled $M_2 - M_1$, $M_3 - M_1$ and $M_3 - M_2$ are equal to the differences between two of three breathers mass $M_n - M_{n'}$ calculated from eq. (7).

Within the framework of the quantum SG field theory, there is no excitation from the ground state that has energy $M_n - M_{n'}$. Thus, these resonance modes can be assigned as the interbreather transitions. As shown in Fig. 4, these interbreather transitions have sufficient intensities as the breathers. The present ESR experiments were done at 0.5 K, at which the population of the excited level is negligible under isothermal condition. At zero magnetic field, however, breathers do not exist, there are gapless modes at $q = 0$ and π , which change to the breathers modes due to the staggered field induced by the external field. The population of the gapless mode at zero magnetic field is finite even at 0.5 K. In the present ESR measurements combined with the pulsed magnetic field with the width of about 10 msec, the splitting of the levels occur under almost adiabatic conditions. Therefore, the population at zero magnetic field is maintained even in finite field and the interbreather transitions can be observed.

As shown in Fig. 5 (b), weak resonance modes labeled C_n with $n = 1, 2$ and 3 were observed for $H \parallel a$ in the fields lower than the field for soliton resonance E_s . These modes are assigned as the multiple excitations of the soliton resonance and the n -th breather, because their energy correspond to $E_s + M_n$. The multiple excitation mode C_1 was also observed for $H \perp (1, 1, 0)$, while for $H \parallel b$ and c , no C mode was observed, which should be ascribed to the large c_s for the latter two field directions. For $H \parallel b$, we observed a resonance mode whose excitation energy is just twice as large as M_1 [19]. This mode can be considered as the simultaneous excitation of two first breathers. This was the first example of the two-breather resonance in the quantum SG spin system. In the present experiments, the two-breather resonance was observed only for $H \parallel b$. In this field direction, we observed as many as twelve modes. The energy of two-soliton excitation $2M_s$ is almost same as the energy of the third breather M_3 . Thus, it is hard to distinguish the $2M_s$ mode from M_3 mode, although the two-soliton excitation is expected to exist.

Resonance modes U_n are unknown modes, whose origins are not clear. The numbering of U_n is in ascending order of excitation energy in each field direction. The field dependence of their energies denoted by thin solid lines in Fig. 5 is similar to that of mass of breathers M_n . In the previous measurements, we also observed the three unknown modes ($U_1 \sim U_3$) for $H \parallel c$ in different specimens. Therefore, the unknown modes should be intrinsic to KCuGaF_6 . Such unknown modes were also observed in another quantum SG system, $\text{PM-Cu}(\text{NO}_3)_2 \cdot (\text{H}_2\text{O})_2$ [11]. However, the origins of these unknown modes are unexplainable within a framework of the quantum SG field theory shown in Section 2.

4.2. Specific heat measurement

In order to study the contribution of elementary excitations to thermodynamic properties, we measured specific heat of KCuGaF_6 . The magnetic field was applied parallel to the c axis, for which the soliton gap is the largest. Figure 7 shows the low-temperature total specific heat C_{total} measured at zero magnetic field. No magnetic ordering was observed down to 0.36 K, which indicates good one-dimensionality of the present system.

C_{total} at zero field exhibits almost linear temperature dependence below 4 K characteristic of the $S = 1/2$ AFHC [21, 22]. C_{total} is composed of magnetic C_{mag} and lattice C_{lattice} contributions. The specific heat of $S = 1/2$ AFHC for $k_B T/J < 0.1$ is approximately given by [21, 22]

$$C_{\text{mag}} = \frac{2Rk_B T}{3J}. \quad (10)$$

In this low temperature region, the Tomonaga-Luttinger (TL) liquid state is realized. The exchange constant in KCuGaF_6 is $J/k_B = 103$ K, which was obtained from the magnetic susceptibility data [16, 19]. Thus, the condition $k_B T/J < 0.1$ is satisfied for $T < 10$ K. The lattice contribution C_{lattice} shown by dashed line in Fig. 7 was obtained by subtracting the T -linear magnetic contribution from the total specific heat C_{total} . The magnetic specific heat in finite magnetic field was obtained by subtracting C_{lattice} from the total specific heat C_{total} .

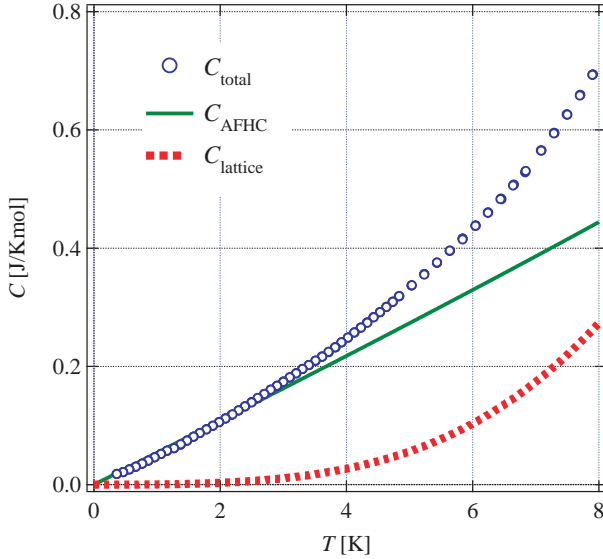


Figure 7: Temperature dependence of specific heat at zero field. Open circles are total specific heat. Solid and dotted lines denote magnetic and lattice contributions, respectively.

Figure 8 shows the low-temperature magnetic specific heat C_{mag} obtained at several magnetic fields applied parallel to the c axis. With increasing temperature, C_{mag} exhibits exponential increase, which indicates the existence of the field-induced gap. With further increasing temperature, C_{mag} displays a rounded shoulder and increases linearly. As magnetic field increases, the shoulder shifts to higher temperature and becomes broader. This shows that the gap increases with applied magnetic field.

Specific heat of the quantum SG model can be obtained by solving a set of integral equations based on the Bethe Ansatz and the $\text{SU}(2)$ symmetry [23, 24], for which the compactification radius is set as $R = 1/\sqrt{2\pi}$. The calculated results were actually in agreement with experimental results in other SG model compounds, Cu benzoate [25] and Yb_4As_3 [12]. When the $\text{SU}(2)$ symmetry is assumed, the mass of the first breather is the same as the soliton mass, i.e., $M_s = M_1 (\equiv \Delta)$. The solid

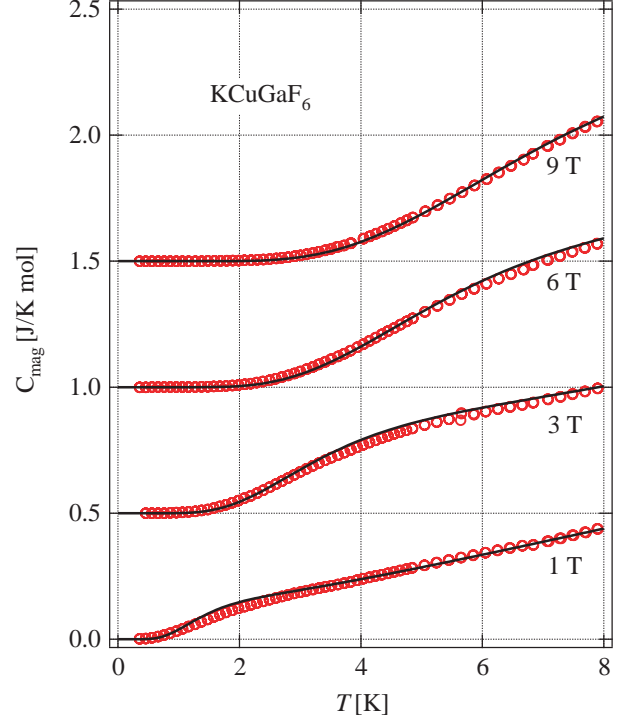


Figure 8: Temperature dependence of magnetic specific heat measured at $H = 1, 3, 6$ and 9 T for $H \parallel c$. Each data is shifted upward by 0.5 J/(K mol). Open circles denote experimental data and solid lines are calculations based on the quantum SG field theory with soliton mass shown in Fig. 9.

lines in Fig. 8 show the theoretical specific heat of the quantum SG model with the $\text{SU}(2)$ symmetry [12], see also Ref. [25]. In this calculation, the adjustable parameter is the gap Δ . The behavior of the magnetic specific heat observed in KCuGaF_6 is well reproduced by the present analysis. With further increasing temperature above 8 K, the discrepancy between the experimental data and fitting curves becomes larger. This is because in such high temperature region, the description by the TL liquid starts to break down.

Figure 9 shows the gap Δ as a function of $H^{2/3}$. It is evident that the gap is described as $\Delta = AH^{2/3}$. The coefficient A is obtained as $A = 5.4$ K/($\text{T}^{2/3}$). This field dependence of the gap is different from the result of the linear spin wave theory, which derives $\Delta \propto H^{1/2}$. From the field for soliton resonance in ESR measurements, we obtained soliton mass indirectly [16, 19]. The soliton mass calculated with eq. (6) and $c_s = 0.18$ for $H \parallel c$ shows the $H^{2/3}$ dependence with proportionality coefficient $A = 4.3$ K/($\text{T}^{2/3}$). The soliton mass obtained from the specific heat result is 1.26 times as large as that obtained from the ESR measurements. The discrepancy may be ascribed to the $\text{SU}(2)$ symmetry, i.e., $\xi = 1/3$, which was assumed for the calculation of the specific heat. When the $\text{SU}(2)$ symmetry is broken by the applied magnetic field, the parameter ξ becomes less than $1/3$. However, eq. (6) gives almost the same soliton mass in our experimental field range. Therefore, only from the $\text{SU}(2)$ symmetry, we cannot explain the discrepancy between soliton masses evaluated from ESR and spe-

cific heat measurements. The presence of the unknown modes, $U_1 - U_3$, which are not explainable in terms of the simple quantum SG model, may also be responsible for the discrepancy. At present, we have no clear explanation about the discrepancy. Anyhow, in KCuGaF_6 , the considerably large staggered field is induced when subjected in the uniform magnetic field parallel to the c axis.

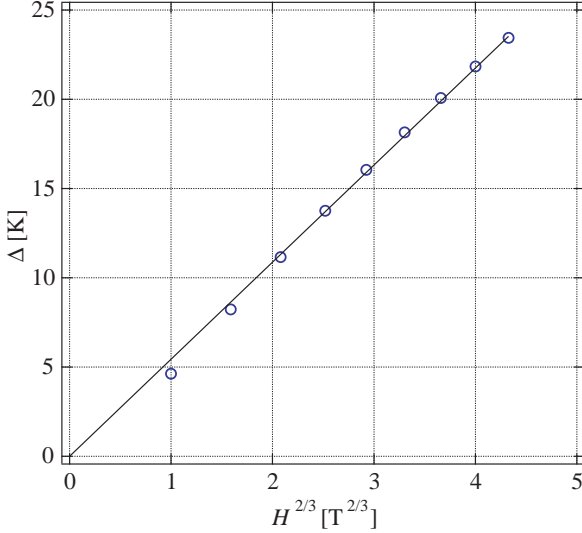


Figure 9: Gap Δ as a function of $H^{2/3}$. Open circles denote the gaps obtained from specific heat measurements for $H \parallel c$. Solid line is a linear fit.

5. Conclusion

In conclusion, we have presented the results of ESR measurement and the specific heat measurements on $S = 1/2$ AFHC KCuGaF_6 with the large exchange interaction $J/k_B = 103$ K. In KCuGaF_6 , the staggered magnetic field h is induced perpendicular to the external magnetic field H owing to the DM interaction with alternating \mathbf{D} vectors and the staggered g tensor. Thus, the present system can be represented by the quantum SG model in a magnetic field. In the present high-frequency ESR measurements combined with pulsed high magnetic field, breathers up to the third order and soliton resonance concerning with soliton mass were directly observed. The energies of these elementary excitations are in good agreement with the calculations based on the quantum SG field theory with a single adjustable parameter $c_s = h/H$. The proportionality coefficient c_s varies widely from 0.03 to 0.18, depending on the field direction. We also observed additional modes, i.e., inter-breather transitions, multiple excitations, and unknown modes that have no clear explanation for their origin.

We measured specific heat for $H \parallel c$, where the gap is the largest. The specific heat shows the evidence of the field-induced gap, which corresponds to the soliton gap at incommensurate wave vector q_0 and the breather gap at $q = 0$ and π . We analyzed the temperature dependence of specific heat, using the SG field theory based with $\text{SU}(2)$ symmetry. We found

that the gap is almost proportional to $H^{2/3}$, as predicted by the SG field theory. Thus, we can conclude that the quantum SG model gives a good description of the elementary excitations in KCuGaF_6 . Details of the present work on specific heat will be published elsewhere [26].

Acknowledgment

This work was supported by a Grant-in-Aid for Scientific Research (A) from the Japan Society for the Promotion of Science, and by a Global Center of Excellence Program “Nanoscience and Quantum Physics” at Tokyo Tech and a Grant-in-Aid for Scientific Research on Priority Areas “High Field Spin Science in 100 T”, both funded by the Japanese Ministry of Education, Culture, Sports, Science and Technology.

References

- [1] L. Hulthén, Arkiv Mat. Astron. Fys. 26A (1938) 1.
- [2] J. des Cloizeaux, J. J. Pearson, Phys. Rev. 128 (1962) 2131.
- [3] R. B. Griffiths, Phys. Rev. 133 (1964) A768.
- [4] N. Ishimura, H. Shiba, Prog. Theor. Phys. 57 (1977) 1862.
- [5] M. Oshikawa, I. Affleck, Phys. Rev. Lett. 79 (1997) 2883.
- [6] I. Affleck, M. Oshikawa, Phys. Rev. B 60 (1999) 1038, Errata, Phys. Rev. B 62 (2000) 9200.
- [7] D. C. Dender, P. R. Hammar, D. H. Reich, C. Broholm, G. Aeppli, Phys. Rev. Lett. 79 (1997) 1750.
- [8] T. Asano, H. Nojiri, Y. Inagaki, J. P. Boucher, T. Sakon, Y. Ajiro, M. Motokawa, Phys. Rev. Lett. 84 (2000) 5880.
- [9] H. Nojiri, Y. Ajiro, T. Asano, J. P. Boucher, New J. Phys. 8 (2006) 218.
- [10] R. Feyerherm, S. Abens, D. Günther, T. Ishida, M. Meißner, M. Meschke, T. Nogami, M. Steiner, J. Phys.: Condens. Matter 12 (2000) 8495.
- [11] S. A. Zvyagin, A. K. Kolezhuk, J. Krzystek, R. Feyerherm, Phys. Rev. Lett. 93 (2004) 027201.
- [12] M. Oshikawa, K. Ueda, H. Aoki, A. Ochiai, M. Kohgi, J. Phys. Soc. Jpn. 68 (1999) 3181.
- [13] R. Matysiak, G. Kamieniarz, P. Gegenwart, A. Ochiai, Phys. Rev. B 79 (2009) 224413.
- [14] In general, the anisotropy of the g tensor and the magnitude of the \mathbf{D} vector of the Dzyaloshinsky-Moriya interaction in fluoride are larger than those in oxide, chloride and bromide, for g tensor, see S. Sasaki, N. Narita, I. Yamada, J. Phys. Soc. Jpn. 64 (1995) 2701. It is considered that the mixing between the d orbital of magnetic ion and the p orbital of anion is smaller in fluoride than in the oxide and the other halide, so that the reduction of the nondiagonal elements of the angular momentum of the d orbital $\langle e | L^{\mu} | g \rangle$ is smaller in fluoride. This leads to the large anisotropy of the g tensor and the large \mathbf{D} vector.
- [15] P. Dahlke, J. Pebler, D. Babel, Z. Anorg. Alleg. Chem. 631 (2005) 115.
- [16] R. Morisaki, T. Ono, H. Tanaka, H. Nojiri, J. Phys. Soc. Jpn. 76 (2007) 063706.
- [17] F. H. L. Essler, A. Furusaki, T. Hikihara, Phys. Rev. B 68 (2003) 064410.
- [18] T. Hikihara, A. Furusaki, Phys. Rev. B 61 (2000) 9558.
- [19] I. Umegaki, T. Ono, H. Tanaka, H. Uekusa, H. Nojiri, Phys. Rev. B 79 (2009) 184401.
- [20] In the classical picture, the motion of the total magnetization corresponding to the soliton resonance is the precession around the external field H , and that for the breather is the oscillation parallel to H .
- [21] A. Klümper, Eur. Phys. J. B 5 (1998) 677.
- [22] D. C. Johnston, R. K. Kremer, M. Troyer, X. Wang, A. Kluemper, S. L. Bud'ko, A. F. Panchula, P. C. Canfield, Phys. Rev. B 61 (2000) 9558.
- [23] C. Destri, H. J. de Vega, Nucl. Phys. B 438 (1995) 413.
- [24] M. Fowler, X. Zotos, Phys. Rev. B 25 (1982) 5806.
- [25] F. H. L. Essler, Phys. Rev. B 59 (1999) 14376.
- [26] I. Umegaki, T. Ono, H. Tanaka, M. Oshikawa, K. Sakai, (Unpublished)